Supporting Information

Efficient elimination of Hg(II) from water bodies with acid-modified magnetic biomass spent tea leaves: Conditional optimization and application

Dingli Cheng [1,ξ], **Yiwen Li** [1,ξ], **Xinyu Zheng** [1], **Yongfu Guo** [1,2]*

[1] School of Environmental Science and Engineering, Suzhou University of Science and Technology, Suzhou, 215009, China

[2] Jiangsu Collaborative Innovation Center of Technology and Material of Water Treatment, Suzhou 215009, Jiangsu, China

[ξ] These authors contributed equally to this work.

[*] Corresponding author: Tel: +86 512 68092987 (Y. Guo).

E-mail address: yongfuguo@163.com (Y. Guo)

1. Materials and instruments

Sodium hydroxide (NaOH, AR, 96%), nickel chloride ($NiCl_2 \cdot 6H_2O$, AR, 99%), ferrric chloride ($FeCl_3 \cdot 6H_2O$, AR, 99%), ammonia (25 – 28 wt.%), potassium chloride (KCl, AR, 99.5%) and humic acid (FA ≥ 90%) were purchased from Macleans (Shanghai, China). Hydrochloric acid (HCl, AR, 37%) and nitric acid (HNO_3, AR, 68%) were purchased from Shanghai Lianshi Chemical Reagent co., LTD., (Shanghai, China). Sodium sulfate (AR, ≥ 99%), urea (AR, 99%), mercury chloride (AR, 99%) and sodium chloride (AR, ≥ 99.5%) were purchased from Sinopharm Chemical Reagent Co., Ltd., (Beijing, China). All of the chemicals are analytical reagent.

Digital display mechanical mixer (OS20-S) and Thermostat Magnetic stirrer (MS-H-Pr) were purchased from Dragon (Shanghai, China). Muffle burner was purchased from Kejing (KSL-1400X-A2, Heifei, China). Cold atomic absorption mercury meter was purchased from Huaguang (F732-VJ, Shanghai, China). Constant temperature drying box was purchased from Jinghong (DHG-9076A, Shanghai, China). Constant temperature water bath rocking bed was purchased from Zhicheng (ZWY-110X30/50, Shanghai, China). Water Purifier (ZRXQ015TQ) was purchased from Milli-Q (USA). Electronic balance was purchased from Sartorius (MSE524S-100-DA, Germany).

2. Samples characterizations

The morphology and structure character of prepared adsorbent $NiFe_2O_4$/STLS were characterized through Scanning Electron Microscope (SEM, Quanta FEG250, FEI, USA), X-ray diffractometer (XRD, Rigaku Ultimate IV, Japan), Fourier Transform Infrared (FT-

IR, Nicolet iN10, Thermo Scientific, USA). The Brunauer-Emmett-Teller (BET) specific surface area was conducted by automatic specific surface and porosity analyzer (BET, ASAP 2020, Micromeritics, USA), and the pore size distribution was determined by desorption isotherm via the Barret-Joyner-Halender (BJH) method.

The X-ray photoelectron spectroscopy (XPS) was used to detect the surface composition, the valence state information and superficial chemical bond state of prepared samples, which was conducted on an X-ray Photoelectron Spectroscopy (XPS, K-Alpha, Thermo Scientic, USA). The magnetic strength of $NiFe_2O_4$/STLS was measured by a Vibrating Sample Magnetometer (VSM, Qunantumpesign, MPMS3, USA). The property of charges on the $NiFe_2O_4$/STLS was determined via a Zeta potentiometer (Zeta PALS, Brookhaven, USA). The Material quality change data was obtained using thermogravimetric analysis (TGA, NETZSCH STA 449F3, Germany)

3. Influence of pyrolysis temperature

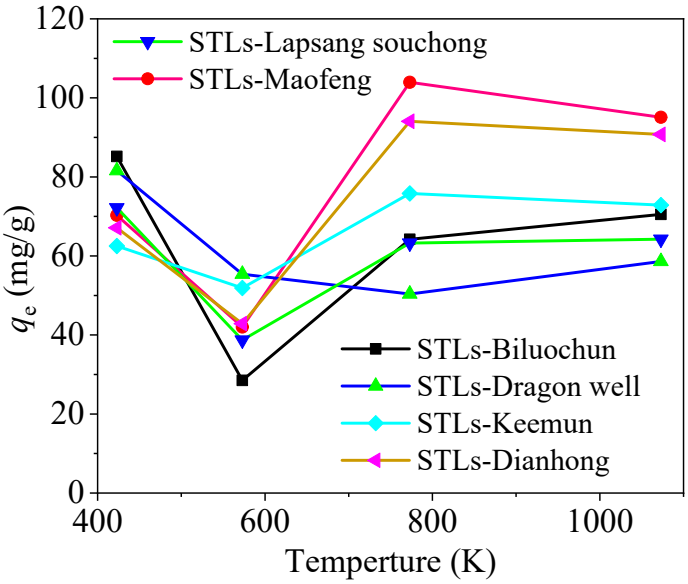

Fig. S1. Influence of pyrolysis temperature.

4. Preparation schematic of $NiFe_2O_4$/STLs

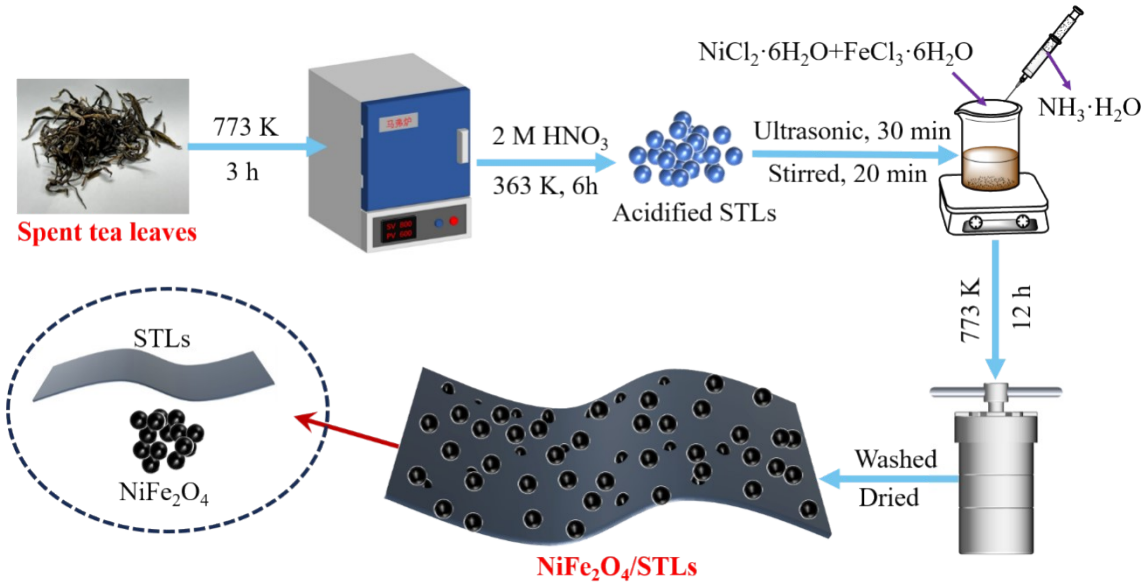

Fig. S2. Schematic diagram of $NiFe_2O_4$/STLs preparation.

5. BET

Fig. S3 is the distributions of adsorption-desorption and pore size of STLs and $NiFe_2O_4$/STLs, and the corresponding data is presented in Table S1.

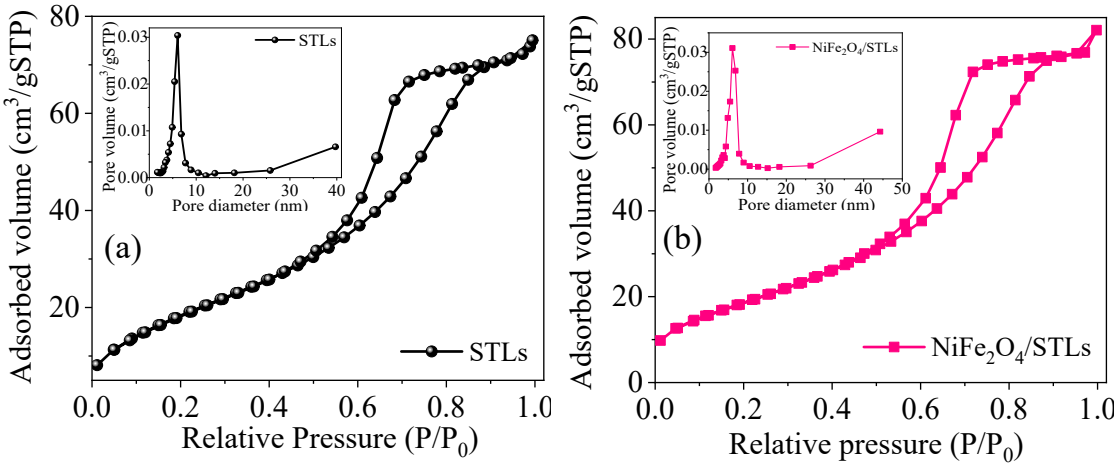

Fig. S3. Isotherm plots and pore size distribution of STLs (a), $NiFe_2O_4$/STLs (b).

From Fig. S3a, there is almost no pore on the STLs surface, but after acid modification and co-precipitation with magnetic nanoparticles of $NiFe_2O_4$, the adsorption capacity towards N_2 over STLS is greatly increased (Fig. S3b), which is in accord

with the change of the isothermal data in Table S1. After acid modification and loading with magnetic nanoparticles, the isothermal data of STLs material, including pore volume and pore size, are greatly enlarged, which is conducive to the promotion of adsorption capacity towards Hg(II).

In addition, the adsorption-desorption curve of $NiFe_2O_4$/STLs is a typical type-IV isotherm. The curve rises upward in low P/P_0 region and the adsorption of N_2 begins to increase rapidly. In the high P/P_0 region, capillary condensation occurs in $NiFe_2O_4$/STLs material, leading to an obvious H3 type hysteresis loop[1, 2]. It can be further speculated that there are certain mesoporous in $NiFe_2O_4$/STLs material, which is consistent with the results of its particle size distribution map shown in Fig. S3a and S3b (the inserted picture). The pore size of $NiFe_2O_4$/STLs is relatively small, mostly distributed between 3 - 8 nm, and essentially the same as STLs. Hence, the as-prepared $NiFe_2O_4$/STLs belongs to magnetic mesoporous composite material.

After recombination with magnetic particles $NiFe_2O_4$, the surface of STLs is covered by magnetic nanoparticles, resulting in a relative reduction in the specific surface area and an increase in total pore capacity.

Table S1. Isothermal data of STLs and $NiFe_2O_4$/STLs.

Samples	BET (m^2/g)	Pore volume (cm^3/g)	Pore size (nm)
STLs	71.87	0.116	6.461
$NiFe_2O_4$/STLs	68.28	0.127	7.437

6. RSM optimization results

Table S2. RSM optimization results of $NiFe_2O_4$/STLs.

Std.	Runs	Variables				q_e (mg/g)
		pH (A)	C_0 (B)	T (C)	Dosage (D)	
24	1	8	20	30	0.09	182.94
22	2	8	40	30	0.09	204.1
20	3	7	10	35	0.1	152.6
3	4	6	40	40	0.09	140.4
2	5	6	40	30	0.09	173.2
14	6	7	30	35	0.1	196
11	7	7	50	35	0.1	178.9
30	8	9	30	35	0.1	164.6
17	9	7	30	35	0.1	195
18	10	7	30	35	0.1	190
21	11	7	30	35	0.12	160.26
15	12	7	30	35	0.1	191
28	13	8	20	30	0.11	181.4
12	14	7	30	25	0.1	171.2
16	15	7	30	35	0.1	194
6	16	6	40	30	0.11	167.6
1	17	5	30	35	0.1	119.8
19	18	7	30	45	0.1	136.5

Std.	Runs	Variables				q_e (mg/g)
		pH (A)	C_0 (B)	T (C)	Dosage (D)	
8	19	6	20	30	0.11	159.2
29	20	8	20	40	0.11	152.74
26	21	8	40	30	0.11	187.4
5	22	6	20	40	0.09	119.34
23	23	8	40	40	0.09	169
4	24	6	20	30	0.09	148
10	25	7	30	35	0.08	171.6
25	26	8	20	40	0.09	147.96
7	27	6	40	40	0.11	136
13	28	7	30	35	0.1	199
27	29	8	40	40	0.11	155.42
9	30	6	20	40	0.11	136.76

Table S3. Calculated results of four models.

Models	Std. Dev	R^2	Adjusted R^2	Predicted R^2	Press.	
Linear	17.43	0.5346	0.4602	0.4174	9512.3	
2FI	19.32	0.5656	0.3370	0.3013	11407.82	
Quadratic	5.16	0.9756	0.9528	0.9239	2059.52	Suggested
Cubic	3.93	0.9934	0.9728	0.5240	7771.65	

Table S4. ANOVA analysis of Quadratic model.

Source	Sum of Squares	df	Mean square	F-value	P-value	
Model	15928.20	14	1137.73	240.89	＜0.0001	Significant
A-pH	3505.62	1	3505.62	131.90	＜0.0001	
B-C0	4150.67	1	4150.67	156.17	＜0.0001	
C-T	1032.02	1	1032.02	99.21	＜0.0001	
D-Dosage	40.30	1	40.30	1.52	0.2371	
AB	14.48	1	14.48	0.5447	＜0.0001	
AC	0.57	1	0.57	0.0214	＜0.0001	
AD	130.3	1	130.3	4.9	＜0.0001	
BC	17.51	1	17.51	0.659	＜0.0001	
BD	17.77	1	17.77	0.6684	＜0.0001	
CD	325.26	1	325.26	12.24	0.0032	
A^2	4261.89	1	4261.89	160.35	＜0.0001	
B^2	2502.97	1	2502.97	94.17	＜0.0001	
C^2	1186.73	1	1186.73	44.65	＜0.0001	
D^2	1170.55	1	1170.55	44.04	＜0.0001	
Residual	398.68	15	26.58			
Lack of Fit	343.85	10	34.38	3.14	0.1095	Insignificant
Pure Error	54.83	5	10.97			
Cor Total	16326.88	29				

7. Effect of adsorbent dosage

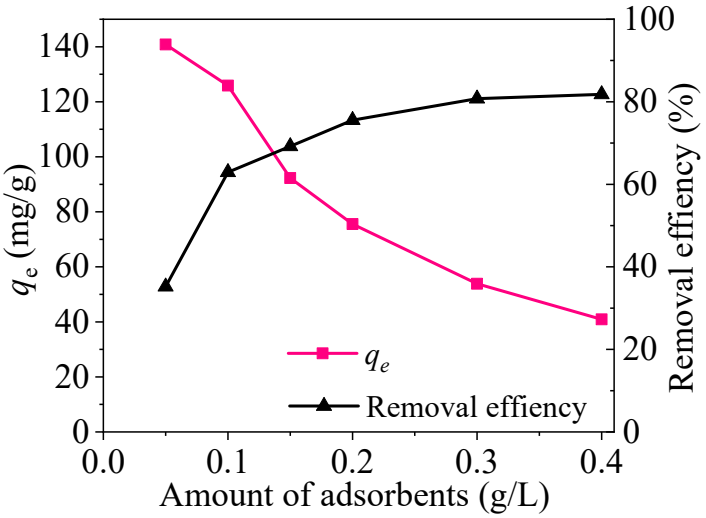

Fig. S4. Effect of dosage on Hg(II) removal. Conditions: dosage = 0.05 – 0.4 g/L, C_0 = 20 mg/L, T = 298 K, reaction time t = 24 h, solution volume V = 100 mL, pH = 8.

From Fig. S4, the increase of adsorbent dosage can significantly improve the removal rate of Hg(II). With the addition of dosage rising from 0.05 g/L to 0.4 g/L, the Hg(II) removal rate increases from 22.5% to 85.8%. However, the adsorption capacity of $NiFe_2O_4$/STLS towards Hg(II) decreases from 140.85 mg/g to 40.91 mg/g. It indicates that as the $NiFe_2O_4$/STLS dosage increases, although the overall adsorption active sites increase and more effectively removal of Hg(II) has been achieved, the adsorption saturation occurs and active sites are gradually occupied. Meanwhile, condensation occurs on the adsorbent surface. Hence, under the high dosage, the mercury removal rate has instead decreased.

Considering the adsorption amount and adsorption efficiency of $NiFe_2O_4$/STLS towards Hg(II), the dosage of 0.1 g/L was selected as the optimal adsorbent amount of the subsequent experiments.

Table S5. Comparison of adsorption capacity of Hg(II) with reported adsorbents.

Adsorbents	BET (m^2/g)	pH	T (°C)	Kinetic fitting models	Isotherm fitting models	Thermodynamics	Q_m (mg/g)	Ref.
MWCNTs-COOH	97	7.8	25	Pseudo-first-order	Langmuir	$\Delta H^0 > 0$，$\Delta G^0 < 0$	91.74	[3]
Biochar with 3-MPTS	—	7	—	Pseudo-second-order	Langmuir	—	126.62	[4]
MNP-CD-PBTCA	13.84	4	55	Pseudo-second-order	Langmuir	$\Delta H^0 > 0$，$\Delta G^0 < 0$	77.59	[5]
$CoFe_2O_4$@mSiO_2-NH_2	17.08	7	25	Pseudo-second-order	Langmuir	$\Delta H^0 < 0$，$\Delta G^0 < 0$	149.3	[6]
Ball-milled biochar 700	296.3	5	45	Intra-particle diffusion	Langmuir	$\Delta H^0 > 0$，$\Delta G^0 < 0$	127.4	[7]
E-ZFA-Ag	128.7	2.5	2.5	-	Langmuir	—	107.4	[8]
Humic acid/biochar	2.85	—	55	Pseudo-second-order	Freundlich	—	38.33	[9]
Boehmite@Fe_3O_4@PLA@SiO_2	—	7	25	Pseudo-second-order	Langmuir	—	36.94	[10]
Elatin@SiO_2	675.92	6	40	Pseudo-second-order	Langmuir	$\Delta H^0 > 0$，$\Delta G^0 < 0$	43.85	[11]
CNFs/GO/Fe_3O_4	55	7	25	Pseudo-second-order	Langmuir	—	36.70	[12]
$NiFe_2O_4$/STLS	68.28	8	39	Pseudo-second-order	RSM	$\Delta H^0 < 0$，$\Delta G^0 < 0$	204.42	This work
$NiFe_2O_4$/STLS	68.28	8	35	Pseudo-second-order	Langmuir	$\Delta H^0 < 0$，$\Delta G^0 < 0$	189.64	This work

8. Water quality parameters of actual water samples

Table S6. Water quality of Biyu river, lake water and effluent of sewage treatment plant.

Water quality	Biyu river	Lake water	Effluent of sewage treatment plant
COD_{Mn} (mg/L)	20.91	19.45	24.51
BOD_5 (mg/L)	2.03	2.49	3.02
TN (mg/L)	4.12	5.35	6.38
TP (mg/L)	0.21	0.11	0.15
TOC (mg/L)	4.01	3.31	2.45
Ammonia nitrogen (mg/L)	0.71	0.82	0.64
pH	7.16	7.63	7.45
Conductivity (μS/cm)	420.12	460.05	680.26

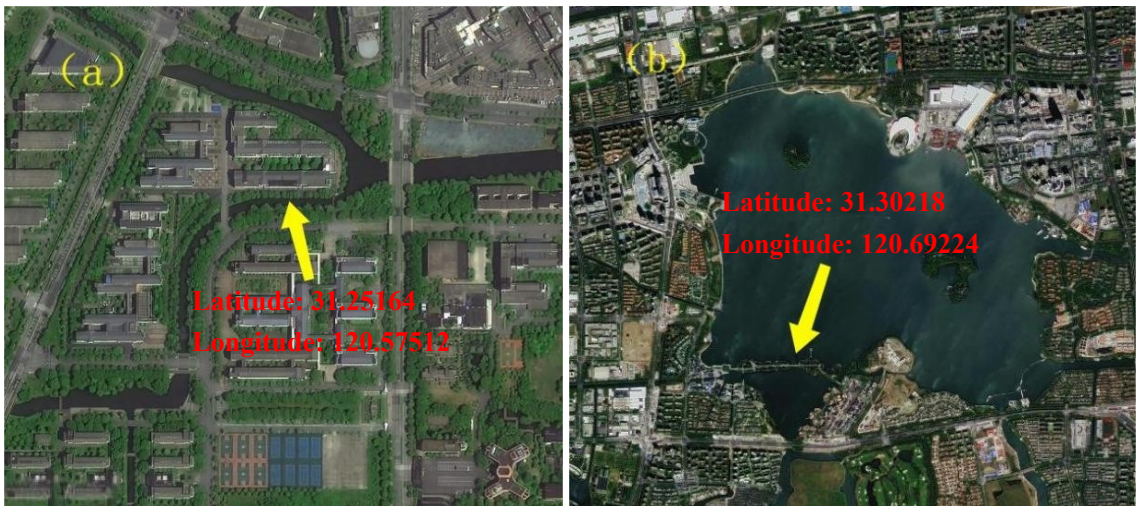

Fig. S5. Sample location of Biyu river (a) and lake water in Suzhou city (b).

9. Regeneration

To test the potential of composite material $NiFe_2O_4$/STLS in practical application, 0.1 mol/L HCl was used as the regenerative agent. The spent material of 0.2 g/L was placed in the above acidic environment for 4 h with ultrasonic vibration at 298 K, then was separated by external magnetic field, washed with pure water and dried. The treated regenerative adsorbent was reused for the next mercury adsorption, and the process was repeated a certain time to evaluate the regenerative performance of composite adsorbent $NiFe_2O_4$/STLS.

As shown in Fig. S6, the adsorption capacity of $NiFe_2O_4$/STLS towards Hg(II) achieves 103.82 mg/g after five adsorption-desorption cycles. Accordingly, the adsorption capacity decreases by only 13.5%. After 8 cycles, the adsorption capacity towards Hg(II) still obtains 94.81 mg/g. The results indicate that the prepared adsorbent has good recyclability.

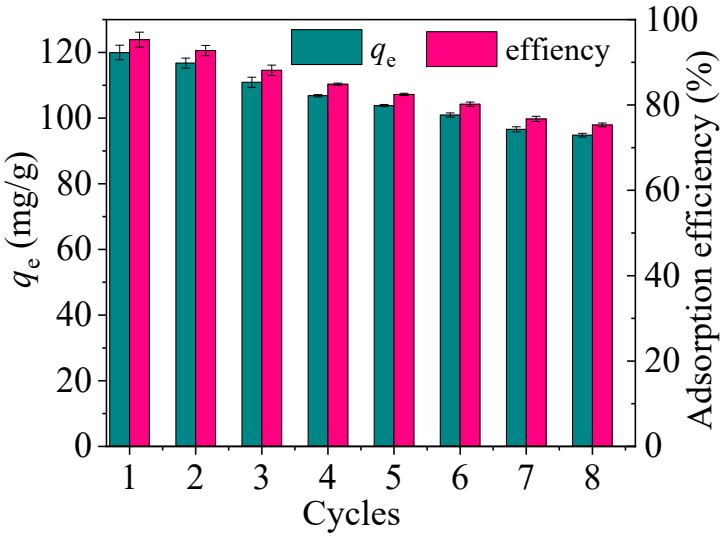

Fig. S6. Regeneration cycles of $NiFe_2O_4$/STLS.

10. Models of adsorption kinetics

Pseudo-first-order model:

$$\ln\left(q_e - q_t\right) = lnq_e - K_1 t \tag{S1}$$

If $\log(q_e - q_t)$ is plotted against t and a straight line is obtained, the adsorption conforms to the pseudo-first-order model. In many cases, the pseudo-first-order model is not consistent with the experimental data for the whole adsorption time and is only suitable for the initial stage of the adsorption process.

Pseudo-second-order model:

$$\frac{t}{q_t} = \frac{1}{K_2 {q_e}^2} + \frac{t}{q_e} \tag{S2}$$

If t/q_t is plotted against t to obtain a straight line, the adsorption process conforms to the pseudo-second-order model. The larger the value of q_e and K_2, the faster the adsorption rate, and the adsorption is easy to reach equilibrium.

Intra-particle diffusion model:

$$q_t = K_d t^{1/2} + C \tag{S3}$$

The slope of the straight part is the diffusion rate constant K_d. The intercept can represent the boundary layer thickness, that is, the larger the intercept, the thicker the boundary layer.

Elovich model:

$$q_t = \frac{1}{\beta} ln(\alpha\beta) + \frac{1}{\beta} lnt \tag{S4}$$

Elovich equation can be applied to the process where the activation energy varies greatly during the reaction.

Two constant equation:

$$lnq_t = lnA + Blnt \tag{S5}$$

The Two constant equation, also known as Freundlich modified formula, can describe the heterogeneity of the energy distribution on the adsorbent surface, and is also suitable for the more complex kinetic equation of the reaction process.

here, q_e (mg/g) is the equilibrium adsorption capacity; q_t (mg/g) is the adsorption capacity at time t (min); k_1 (min^{-1}), k_2 (mg/(g·min)) and k_d (mg/(g·$min^{0.5}$)) are the rate constants of the pseudo-first order, the pseudo-second order and intra-particle diffusion model, respectively; α (mmol/g·min^{-1}) and β (g/mmol) are the constants of Elovich, representing the initial adsorption rate constant and desorption rate constant, respectively; A and B are rate constants and C (mg/g) is the boundary layer thickness.

11. Models of adsorption isotherms

The Langmuir model is suitable for monolayer adsorption of homogeneous surface sites. The Freundlich model is suitable for multilayer adsorption on heterogeneous surfaces. The Temkin model considers the interaction between adsorbent and adsorbent. The Dubinin-Radushkevich (D-R) model is used to determine whether the adsorption property is physical or chemical adsorption.

Langmuir model:

$$\frac{C_e}{q_e} = \frac{C_e}{q_m} + \frac{1}{q_m K_L} \tag{S6}$$

$$R_L = (1 + K_L C_0)^{-1} \tag{S7}$$

The R_L value can be used to indicate whether the isotherm is of favorable ($0 < R_L <$

1), linear ($R_L = 1$), unfavorable ($R_L > 1$), or irreversible form ($R_L = 0$).

Freundlich model:

$$q_e = K_F C_e^{\frac{1}{n}} \tag{S8}$$

1/n is a heterogeneous factor characterizing the adsorption capacity and strength. When the value of 1/n is between 0 and 1, it indicates that the adsorption is feasible and easy. When 1/n = 1, the adsorption is linear, indicating that there is no interaction between adsorbent and adsorbent. When the value is greater than 1, the adsorption is negative and the adsorption is very difficult.

Temkin model:

$$q_e = \frac{RT}{b_T} \ln\left(k_T C_e\right) \tag{S8}$$

D-R model:

$$q_e = q_m e^{-\beta\varepsilon^2} \tag{S9}$$

$$E = \frac{1}{\sqrt{2\beta}} \tag{S10}$$

Hill model：

$$E = \frac{q_{SH} \times C_e \times n_H}{k_D + C_e \times n_H} \tag{S11}$$

When the E value is in the range of 8 to 16 kJ·mol^{-1}, the adsorption is chemisorption. Less than 8 kJ·mol^{-1} was considered as physical adsorption.

Where q_e and q_m (mg/g) are the equilibrium and the maximum adsorption amount, respectively; K_L, K_F, *and* K_T represent the Langmuir, Frendlich and Temkin constants,

which are related to the adsorption energy and adsorption capacity; C_e (mg/g) denotes the equilibrium concentration; n is the parameter of the Freundlich model and depended on temperature, which relates to the adsorption performance of the adsorbent; R (8.314 $J \cdot mol^{-1} K^{-1}$) is the gas constant; T is the Kelvin temperature (K); β ($mol^2 \cdot J^{-2}$) is a constant related to the mean energy of adsorption; ε ($kJ^2 \cdot mol^{-2}$) is the Polanyi potential, which can be obtained from $\varepsilon = RT \ln(1+1/C_e)$; E ($kJ \cdot mol^{-1}$) is the mean free energy and b_T (KJ/mL) is the Temkin constant. q_{SH} is the Hill isotherm maximum uptake saturation (mg/L). k_D is the Hill constant and n_H is the Hill cooperativity coefficient of the binding interaction.

12. Models of adsorption thermodynamics

Thermodynamics parameters such as the Gibbs free energy change (ΔG^0), entropy change (ΔS^0), and enthalpy change (ΔH^0), were calculated according to the following equations:

$$\Delta G^0 = -RT ln K_R \tag{S12}$$

$$ln K_R = \frac{\Delta S^0}{R} - \frac{\Delta H^0}{RT} \tag{S13}$$

$$\Delta G^0 = \Delta H^0 - T\Delta S^0 \tag{S14}$$

where, R (8.314 J/(mol·K)) is the ideal gas constant, and T (K) is the temperature in Kelvin. K_R is adsorption distribution coefficient ($K_R = q_e/C_e$). The values of ΔH^0 and ΔS^0 can be obtained from the slope and intercept of the curve $ln(K_R)$ vs. 1/T.

References

1. Qian, L.; Zeng, Z.; Zhang, S. Y.; Xia, K.; Guo, Y. F., *New J. Chem.,* 2021, 45(32), 14724-14738. https://doi.org/10.1039/d1nj02409d

2. Lin, Z. F.; Pan, Z. W.; Zhao, Y. H.; Qian, L.; Shen, J. T.; Xia, K.; Guo, Y. F.; Qu, Z., *Nanomaterials,* 2020, 10(7). 1370. https://doi.org/10.3390/nano10071370
3. Alimohammady, M.; Jahangiri, M.; Kiani, F.; Tahermansouri, H., *Res.* Chem. *Intermediat.,* 2017, 44(1), 69-92. https://doi.org/10.1007/s11164-017-3091-4
4. Huang, Y.; Xia, S.; Lyu, J.; Tang, J., *Chem. Eng. J.*, 2019, 360, 1646-1655. https://doi.org/10.1016/j.cej.2018.10.231
5. Lin, L.; Zou, C., *J. Chem. Eng. Data,* 2017, 62(2), 762-772. https://doi.org/10.1021/acs.jced.6b00827
6. Wang, X.; Zhang, Z.; Zhao, Y.; Xia, K.; Guo, Y.; Qu, Z.; Bai, R., *Nanomaterials,* 2018, 8(9). 673. https://doi.org/10.3390/nano8090673
7. Li, R.; Zhang, Y.; Deng, H.; Zhang, Z.; Wang, J. J.; Shaheen, S. M.; Xiao, R.; Rinklebe, J.; Xi, B.; He, X.; Du, J., *J. Hazard. Mater.,* 2020, 384, 11. https://doi.org/10.1016/j.jhazmat.2019.121095
8. Suleimenova, M.; Zharylkan, S.; Mekenova, M.; Mutushev, A.; Azat, S.; Tolepova, A.; Baimenov, A.; Satayeva, A.; Tauanov, Z., *Int. J. Mol. Sci.,* 2023, 24(14), 16. https://doi.org/10.3390/ijms241411317
9. Zhang, S. S.; Song, J. P.; Du, Q.; Cheng, K.; Yang, F., *Chemosphere,* 2020, 250, 8. https://doi.org/10.1016/j.chemosphere.2020.126606
10. Alinezhad, H.; Zabihi, M.; Kahfroushan, D., *J. Phys. Chem. Solids,* 2020, 144, 13. https://doi.org/10.1016/j.jpcs.2020.109515
11. Jam wal, H. S.; Ranote, S.; Kumar, D.; Chauhan, G. S.; Bansal, M., *Sep. Purif. Technol.,* 2020, 239, 8. https://doi.org/10.1016/j.seppur.2020.116513
12. Hosseini, M.; Dizaji, H. Z.; Taghavi, M.; Babaei, A. A., *Ind. Crop. Prod.,* 2020, 154(13), 112696. https://doi.org/10.1016/j.indcrop.2020.112696